Journal of Medicinal and Nanomaterials Chemistry 1 (2023) 33-52

SPC

Journal of Medicinal and Nanomaterials Chemistry

Journal homepage: https://jmnc.samipubco.com/

Review Article

Hot electron in visible-light-induced plasmonic photocatalysis by AuNP/TiO_2 –A Review

Nasim Kamely *

Department of Physics, National Taiwan University (NTU), Taipei, Taiwan

ARTICLE INFORMATION

Received: 14 January 2023
Received in revised: 19 February 2023
Accepted: 25 February 2023
Available online: 27 February 2023
Checked for Plagiarism: **YES**

DOI: 10.48309/JMNC.2023.1.3

KEYWORDS

Hot electron
Gold nanoparticle (AuNP)
Titanium dioxide (TiO_2)
Plasmon
plasmonic photocatalysis

ABSTRACT

AuNP/TiO_2 nanocomposite is promising for developing visible-light-induced plasmonic photocatalysis. The effective hot electron generation and inhabitation of electron-hole recombination are the paradigms for the efficiency of plasmonic photocatalysis. The photon-energy alteration in AuNP/TiO_2 depends upon the shape, size, TiO_2 phase, and crystallinity, irradiation wavelength, etc. For its movement, there are different suggestions, such as electron-phonon interaction, direct electron transfer, PRET, PIRET, remote activity mechanism, charge transfer mechanism, plasmon heating, Forster resonance energy transfer, etc. Here, such different parameters and various physical mechanisms for its generation and role in the plasmon-induced photocatalysis by AuNP/TiO_2 are being reviewed.

Corresponding author, email: kamelynasim@gmail.com (N. Kamely).

Graphical Abstract

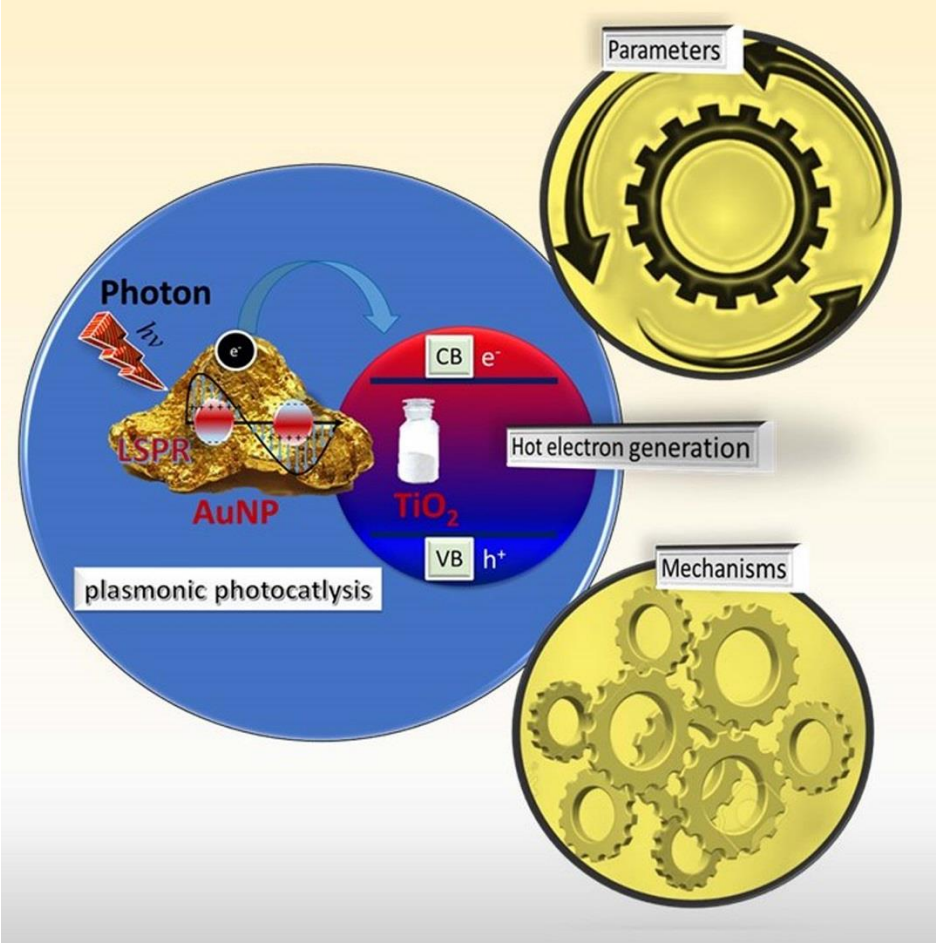

Introduction

'Hot-electron' is a non-equilibrium ensemble of high energy carriers in a semiconductor device [1-5]. Either electrons or holes have gained very high kinetic energy after being accelerated by a strong electric field [6-8]. The excited localized surface plasmon resonance (LSPR) could directly translate the absorbed visible light into electrical energy by hot electron generation [9-15]. Generating hot electrons and preventing charge recombination is the key to effective plasmonic photocatalysis by AuNP/TiO_2 [16-27]. However, the decreased turnover frequency (TOF) due to the recombination of the electrons (e^-) and holes (h^+), acute short lifetime, low migration rates, and uncertain diffusion directions are challenges for its practical applications [28-38]. To address these issues, the hot electrons' production and mechanisms must be properly understood for efficient electron storing, interfacial charge transfer, shuttle process, and synergy between AuNP and TiO_2 [39, 40]. The AuNP/TiO_2 nanocomposite brings a quasi-Fermi level shift inside AuNP to advance the charge separation and raise the interfacial charge transfer process [35, 41]. The hot electrons are accumulated by forming a Schottky barrier between AuNP and TiO_2 heterojunction [11, 35]. The hetero-junction geometry between AuNP and TiO_2 plays a

significant role in the hot electron generation and mobility [42-46]. TiO2's various phases and portions play significant roles in efficient charge transfer and separation. If the amount of TiO_2 on AuNP is moderately lower, it fails to prevent the charge recombination by effective charge separation. If it is substantially higher, a damping effect occurs as the gold nanoparticle is covered with TiO_2 [17]. For the excitation wavelength under visible light, the Schottky barrier between AuNP and TiO_2 barred the movement of the electrons either way, except the LSPR excitation is strong enough to surpass the Schottky barrier [42, 43]. Under ultraviolet (UV) excitation, the photocatalytic activity is dropped as the AuNP works as a charge recombination center [44-49]. The excited hot electrons couple with the phonons and return to the ground state either by scattering the photon or by generating electric charge carriers [50-52].

Thus, it could be seen that adequate hot electron generation and minimization of the electron-hole recombination are the main determinants to control other parameters optimized for superior plasmonic photocatalysis. Yet, with all these, the generation of hot electrons on the AuNP surface and its streaming towards TiO_2 is a subject of debate [53-56]. As this review article sheds light on different parameters and proposals made for generating hot electrons in AuNP/ TiO_2, it would help in understanding the recent progress and factors that affect the plasmonic photocatalysis by AuNP/ TiO_2 and leading to the designing of advanced AuNP/ TiO_2 plasmonic photocatalyst.

AuNP/ TiO_2 geometry and hot electron generation

Comparing the photoluminescence (PL) spectra of TiO_2 and Au-TiO_2 indicates that absorption losses are achieved when AuNPs are at the substrate- TiO_2 interface. An efficient charge transfer leads to efficient electronic interaction between AuNP and TiO_2. The PL spectra for both pure TiO_2 and Au- TiO_2, at 2.0 eV, are due to the interfacial self-trapped electrons. The PL spectra below such optical band gap are associated with e-h+ recombination due to electronic defects (Figure 1) [57]. The difference in photocatalytic activities between different shapes is related to the content of gold in the form of electropositive species (Au^+) and the amount of Ti^{3+} defect centers [58]. For spherical AuNP/ TiO_2, hot electron generation is affected by the surface-to-volume (S/V) ratio [28, 40].

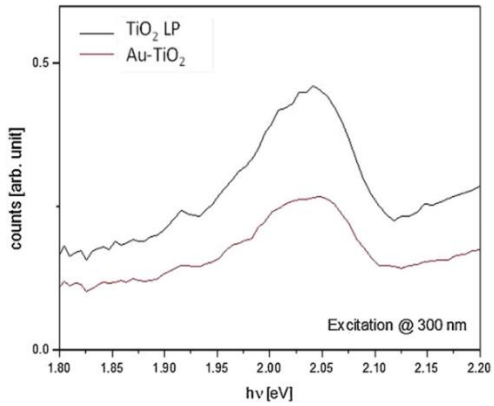

Figure 1. Photoluminescence (PL) spectra TiO_2 and Au-TiO_2 nanoparticles (Adapted with permission from ref. 57 Copyright 2020, Elsevier) [57]

The back reflection is reduced by placing the AuNP at the back of the TiO_2, which is also affected by the morphologies and size of the nanocomposite (Scheme 2) [58, 59]. Au-nanorods, Au- nano bipyramids, and Au triangular excitation wavelength, structure, and shapes are critical factors for hot electrons' relaxation time [60-65]. The lifetime of hot electrons follows the order: of sphere < rod < 3D hierarchical shape [66]. In another study, visible light photoactivity of AuNP with rutile powders TIO-6 (Au-TIO-6) follow the order: nanospheres (NSPs) > (nanorods) NRs > (nanostars) NSTs [58]. If the AuNP surface is asymmetric, the wave propagation length is extended, directing a large portion of the electromagnetic energy from the metal surface to the adjacent dielectric media [67, 68]. For non-radiative 'near-field' activities, the electromagnetic fields govern close to the antenna or scattering object, while 'far-field' characteristic prevails at longer lengths [52]. The density functional theory (DFT) study proposed that the adhesive energy between AuNP and TiO_2 for the defect-rich non-stoichiometric surface is higher and more effective for charge transfer [69-72]. In the quasi-static region, the excitation wavelength is significantly higher than the plasmonic particles, which would cause the optical response to be dipolar and show a Lorentzian line shape close to the resonance frequency. As a result, the nanoantennas are configured in an array which responds consistently with accumulated photocurrent [73]. As a result, nanoparticles with sharp edges (e.g., nanorice, nanostars, bipyramids, dendritic nanorod, nanostars) produce intense hot spots, which lead to several orders with higher sensitivities (Figure 2 and Scheme 1) [74-79]. These nanostructures work as nano-mirrors, and multiple numbers of reflections occur that could increase the mean path of the photon in the nanostructure, raising the capture rate of the photons [35, 80]. The photocurrent generation by dendritic branched Au/TiO_2 is reported to be higher [78]. And, for confeito-like AuNP/TiO_2 nanoantennas, excited resonant plasmons could decay hot electrons over a potential barrier at the interface (Figure 3 and Scheme 2) [80, 81]. For nanotubes, the directional movement of the photogenerated charges takes place and nanorods show larger dephasing time and the plasmonic response could be extended from the visible to the near-infrared wavelength [82, 83]. For dumbbell-shaped Au/TiO_2, the Au as the bar of the dumbbell acts as a photo-anode while the TiO_2 as heads acts as a photo-cathode and an efficient charge transfer takes place [84, 85] (Scheme 3).

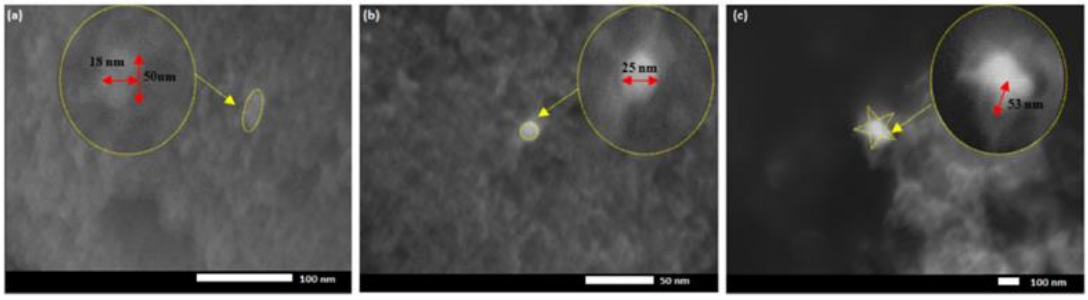

Figure. 2. SEM images of Au-TiO_2: (a) gold nanorods, (b) gold nanospheres, and (c) gold nanostars at the surface of rutile TiO_2 (Adapted with permission from ref. 58 Copyright 2020, Elsevier) [58].

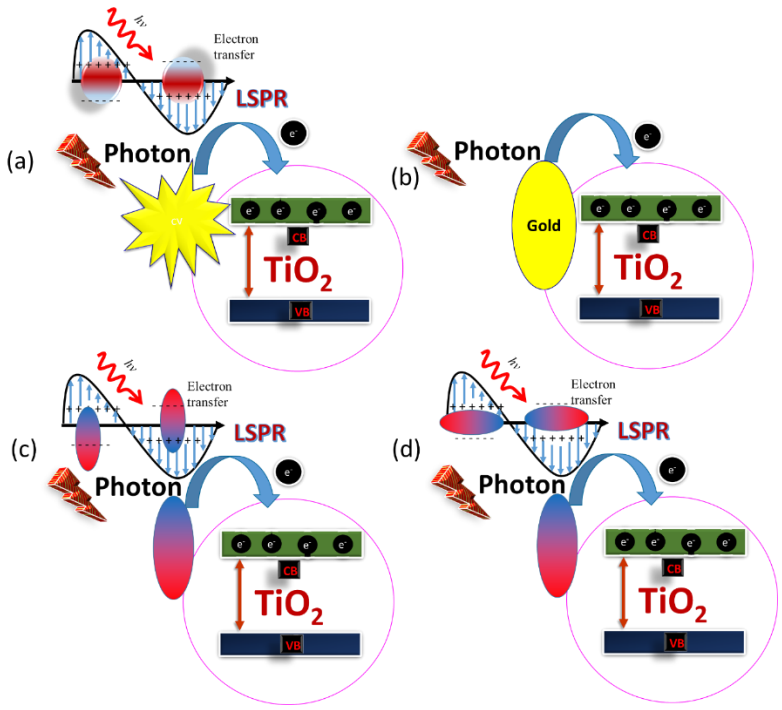

Scheme 1. Effect of gold nanoparticle shapes on Au/TiO_2 excitation under visible light and interaction between TiO_2 matrix and gold nanospheres (a); gold nanostars (b); gold nanorods attached by elongated axis (c); and gold nanorods attached by narrower axis (d) [58]

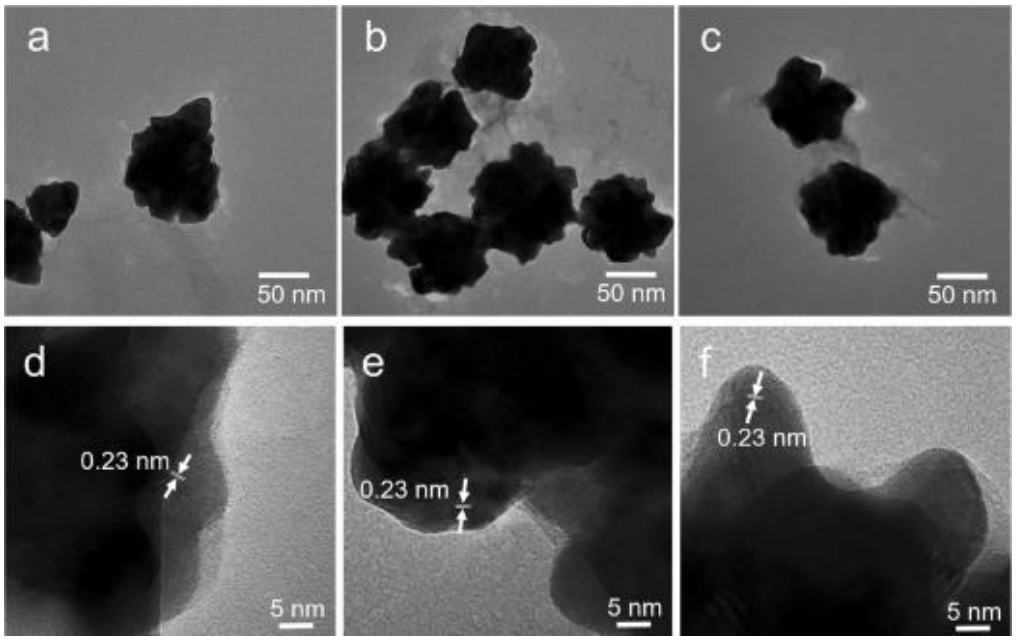

Figure 3 TEM (a–c) and HRTEM images (d–f) of CAuNP/TiO_2 nanocomposite (medium Ti) synthesized for 24 h under different irradiation conditions: a, d in darkness, b, e under visible light, and c, f under UV light (Adapted with permission from ref. 17 Copyright 2020, Springer Nature) [17]

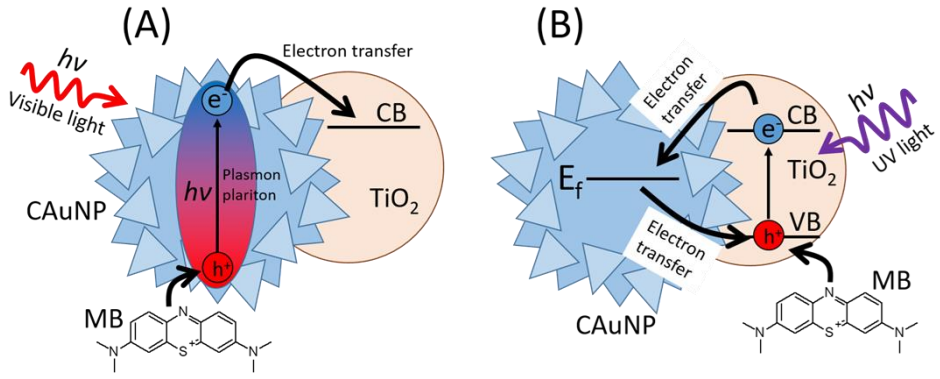

Scheme 2. Degradation mechanism of MB by CAuNP/TiO_2 under visible light (A) and deactivation of TiO_2 under UV irradiation (Adapted with permission from ref. 17 Copyright 2020, Springer Nature) [17]

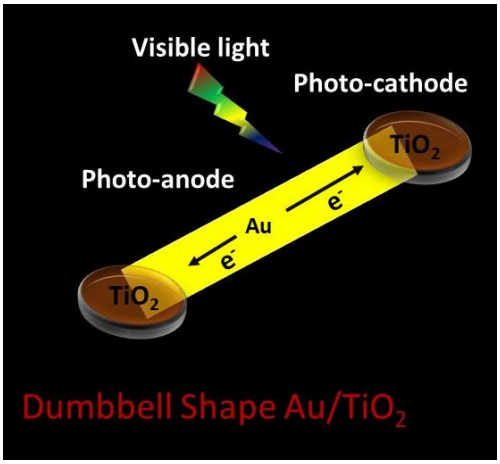

Scheme 3. Dumbbell-shaped Au/TiO_2; the bar performs as photoanode, and the bells act as photocathode [88]

AuNP/doped-TiO_2 and hot electrons

Sandwiching of a redox molecule between AuNP and TiO_2 significantly affects plasmon by blocking the charge recombination process to a more significant extent. Introducing heteroatoms in titania generate additional allowed energy levels inside the wide bandgap. The Additional permitted energy levels in the bandgap stimulate the absorption of visible light photons and introduce an alternative pathway for electron-hole recombination. Hot electron generation is proposed otherwise for differently doped Au/TiO2 [86]. Here one non-metal (nitrogen) and metal (iron) doped Au/TiO_2 is discussed.

The incorporation of N in the TiO_2 lattice in the form of N-O-Ti and Ti-O-N leads to a reduction in bandgap energy (~2.1 eV) by introducing localized states above the valence band. For nitrogen (N), the atomic radius is similar to the oxygen (O), which results in a mixture of Nitrogen 2p and Oxygen 2p to act as an activity source for visible light-generated metastable centers (Scheme 4) [86-89]. Nitrogen 2p states rise to allowed energy states just above the semiconductor's valence band (VB). The 3d states of the metal provide allowed

energy levels near the conduction band (CB). For, both tops of VB and the bottom of CB are broadened due to N doping in TiO_2. , The schottky barrier at the interface, leads to a Fermi level shift to negative potential and increases the interfacial charge transfer process. Interrelationships, whether nitrogen is substitutional and interstitial in the lattice, are not clear; some results suggest that the state of N in titania and its effectiveness in extending the light absorption edge depends upon the preparation methods.

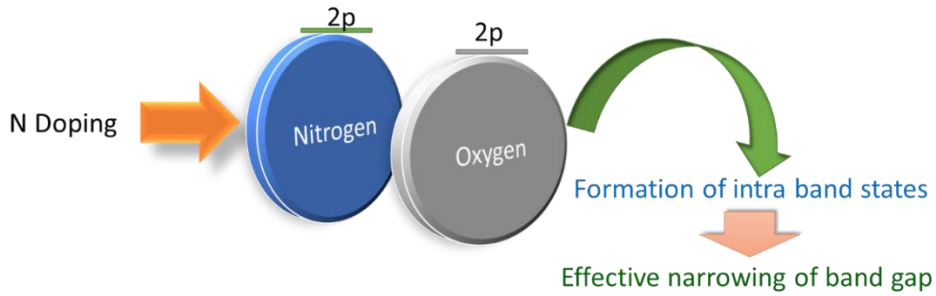

Scheme 4. The mixture of Nitrogen 2p and Oxygen 2p in TiO_2 acts as an activity source for visible light-generated metastable centers

For metal doping, a systematic study with 21 transition metals shows that Fe^{3+}, Mo^{5+}, Ru^{3+}, Os^{3+}, Re^{5+}, V^{4+}, Rh^{3+} photoactivity increases significantly in the liquid-phase degradation of $CHCl_3$, while for Co^{3+} and Al^{3+} doping decreases it [90]. For Au/Fe-TiO_2, PL spectra suggest that the charge recombination rate is inhibited effectively when Au is deposited on the surface of Fe-doped TiO_2 as the e^-s are trapped by AuNP while Fe^{3+} traps the h+s. The addition of Fe^{3+} introduces an impurity level in the bandgap to lead to a lower photocatalytic activity under the UV as the impurity level acts as a recombination center (Scheme 5). Some reports suggest an improved photocatalytic activity for Au/Fe-TiO_2 under visible and UV light by a synergy between AuNP and Fe^{3+} and TiO_2 (Figure 4) [90].

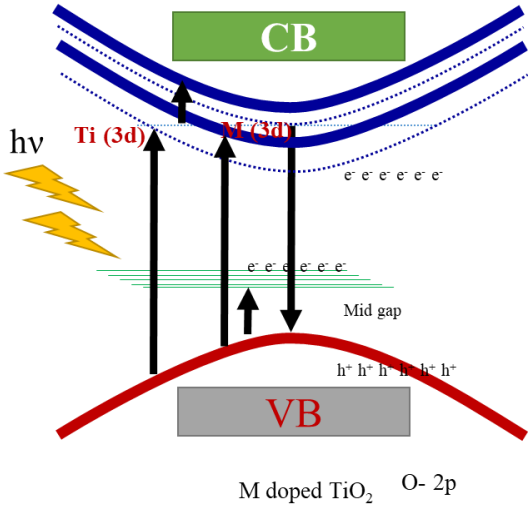

Scheme 5. Band bending for Fe- doped TiO_2; Fe^{3+} introduces an impurity level in the bandgap to lead to a detrimental effect on photocatalytic activity

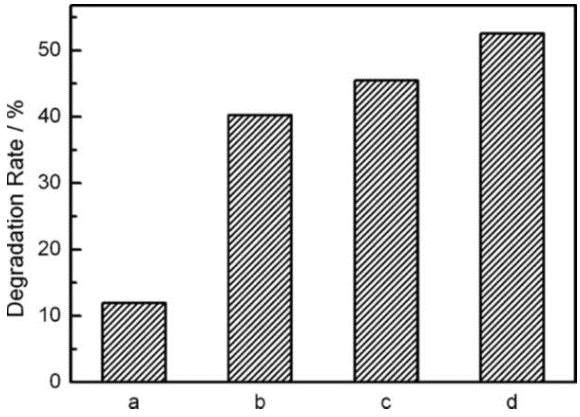

Figure 4 Degradation of methyl orange visible light illumination for 5h over (a) TiO_2, (b) 0.57Fe-TiO_2, (c) 2.0Au/TiO_2, (d) 2.0Au/0.57Fe-TiO_2 (Adapted with permission from ref. 90 Copyright 2020, Elsevier) [90].

Size of AuNP/TiO_2 and hot electron

The apparent Fermi level could be shifted by changing the size of AuNP [91]. Because of discrete energy levels for small-size AuNP, a more significant shift in the Fermi energy level is expected [91]. If the size of AuNP is small enough, the Fermi level of AuNP would be higher than the oxygen due to the quantum size effect and prevent the transfer. For smaller AuNP, the dephasing time becomes prolonged, and plasmon requires an optimum AuNP size for a large dephasing time [92, 93]. For bigger-size AuNP, the Fermi level is lowered, which causes electron transfer from AuNP to TiO_2 [94, 95]. Large size AuNP shorter lifetime result in higher carrier production rates which mostly scatter the incident photons in the forward and backward directions via an absorption/re-emission, whilesmaller nanoparticles trigger near-field enhancement [35, 52]. Some photocatalytic activity tests suggest that the adsorption of dying agents decreases with increasing Au amount, as some adsorption sites are blocked by AuNP. In reports for the degradation of methylene blue (MB) with fixed-sized AuNP, the highest photocatalytic activity was observed when the TiO_2 deposition was 'medium Ti (Ti/Au molar ratio: 0.018), compared to lower (Ti/Au molar ratio: 0.007) and higher Ti (Ti/Au molar ratio: 0.040) (Figure 5) [17].

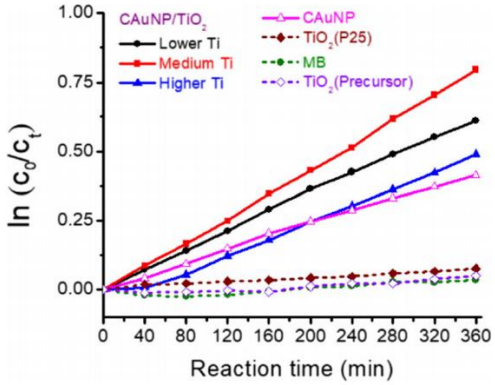

Figure 5. Time course of decomposition rates of MB with CAuNP and CAuNP/TiO2 under visible light (Adapted with permission from ref. 17 Copyright 2020, Springer Nature) [17]

TiO_2 aggregation and hot electron generation

TiO_2 support causes multiple reflections and scattering that increase photon capturing probability [72, 96]. Charge recombination time showed a nonlinear relationship with TiO_2 diameter and diffusion distances for free electrons [97]. Photogenerated charges migrate to the interface when TiO_2 thickness is less than carrier diffusion length (Scheme 6). For a wide TiO_2 layer, internal carriers fail to spread on the surface and tend to recombine [98]. Between AuNP and TiO_2, an optimum ratio is needed for effective plasmon excitation [99, 100].

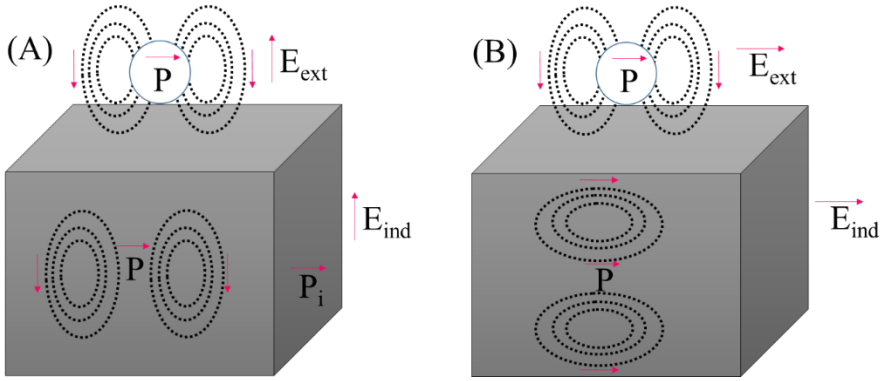

Scheme 6. The exciting field (A) normal to substrate and particle-substrate distance below 1 nm; exciting field strongly modified (B) parallel to the surface; dependence is not obvious

Light wavelengths and hot electron

The incident power variation at a single wavelength results in a linear response with photocurrent, suggesting the photocurrent is dominated by the conversion of single photons to single hot electrons [12, 101]. The work function of Au in a vacuum is ~ 4.78 eV, which tunes the plasmon resonance close to the near-visible region [53, 102]. When LSPR irradiation is done under mixed UV and green light, the hot electrons overcome the Schottky barrier and are transferred from AuNP to TiO_2 under green light. Under UV, these electrons are recompensed from TiO_2 to AuNP and thus accelerate electron-hole recombination [17, 54]. This is significant for the full wavelength application of Au/TiO_2 as the flow of the hot electrons follows the opposite direction to the electron trapping by the Schottky barrier; it could cause a detrimental effect on the photocatalytic activity under the full light spectrum [37, 103]. Some instances also suggest that a small amount of UV with visible light contributes positively tomaking Au particles large enough to enable SPR-promoted electron transfer to the TiO_2 conduction band (CB)' [104].

TiO_2 crystallinity and hot electrons

Both under UV-vis and visible light, the anatase/rutile composites (P25 and Hom) showed more significant activity in H_2 evolution rates due to the electron transfer in both directions across the anatase/rutile interface [105]. Under visible light, no H_2 was evolved with AuNP/anatase- TiO_2 or the anatase/brookite composite. In-situ electron plasmon resonance (EPR) study showed an intrinsic increase of Ti^{3+} in the lattice, which raises the Schottky barrier at the interface and, as a result, hinders SPR-promoted hot electron transfer. This quantum tunneling probability n_i is approached by the modified Fowler theory, which defines the number of "available"

electrons in the system through sufficient energy to overcome the potential barrier:

$$n_i \approx C_F \frac{(h\nu - q\varphi_B)^2}{h\nu} \quad (1)$$

where C_F is the device-specific Fowler emission coefficient, hν is the photon energy and $q\varphi_B$ is the Schottky barrier energy.

Photocatalytic activities of AuNP/anatase-TiO_2 and AuNP/rutile-TiO_2 compared under UV and visible light show that AuNP/anatase-TiO2 had higher activity under the UV-light for the reduction of nitrobenzene than Au/rutile-TiO_2. While under visible light, the Au/rutile-TiO_2 showed superior activity for alcohol oxidation. LSPR favored induced interfacial electron transfer (IET) from AuNP to rutile-TiO_2 due to significant decoupling between the LSPR and inter-band transition modes [106]. The absorption of Ti-OH stretching modes of Au/TiO_2 is in the order of Au/ rutile rods (RR) ≈ Au/3D hierarchical rutile (3DR) < Au/ Anatase rods (RA) ≈ Au/ (Large anatase spheres) LA < Au/(Small anatase spheres) SA and the plasmonic photocatalytic activity under visible light was reported to be the order of Au/SA < Au/P 25 < Au/RA < Au/LA < Au/RR < Au/3DR [69]. It is, therefore, evident that for anatase, the electron transfer takes place through tunneling, while for rutile, it is the direct electron transfer through the contact layer. Discussions of different energy band diagrams between AuNP/anatase-TiO_2 and AuNP/rutile-TiO_2 suggest the Schottky barrier not to be the determining factor for forward electron transfer. At the same time, for the reverse direction, its role is vital to be taken into consideration. The lower photocatalytic performance by Au/SA hetero-structure could be due to the incomplete depletion layer and low band bending. This causes an easy overpass of electrons from TiO_2 CB to AuNP, contributing to faster recombination. For AuNP/rutile-TiO_2, a band shift (~0.294 eV) induces large VB bending, which results in slower charge recombination than anatase-TiO_2 [66].

Again a plot between visible-light activity and AuNP size showed a volcano-shaped curve for Au/rutile-TiO_2, suggesting an optimum size for effective photocatalysis, while for Au/anatase-TiO_2, a rare dependency upon the size of the AuNP was seen [106]. For different crystalline planes, the efficient injection of plasmonic hot electrons is attained by incorporating TiO_2 [001] facets with the AuNP due to the "surface heterojunction". A comparison of Au (111) attached to TiO_2 (110) reconstruction cells displays that it leads to the most stable interfacial configuration for TiO_2 [107].

Mechanisms for hot electrons in AuNP/TiO_2 plasmonic photocatalysis

Electron-photon interaction

For both Plasmon resonance energy transfer (PRET) and scattering effects, the enhancement is observed at the wavelength where the semiconductor resonance and the plasmon resonance overlap. For the hot-electron transfer, the enhancement could occur even at energies below the semiconductor band, which is characteristic of hot electron/hole transfer [50]. The plasmon-excited hot electrons lose coherence rapidly and formulate a non-equilibrium Fermi-Dirac-type distribution through random thermalization by Auger scattering. Besides the formulation of hot electrons through plasmon excitation, incident photons with sufficiently high energies can also cause direct inter-band excitation to the empty d-band of noble metals from the filled sp-band [108]. The energized electrons redistribute energy through a three-step relaxation process:

step I Fermi-Dirac line distribution in less than 1ps through electron-electron (e^--e^-) scattering [11, 109].

Step II Strong electron-photon interaction with electron velocity reduction resulted in metal lattice heating for a few picoseconds [110, 111].

Step III Depending upon the material, particle size, and thermal properties and, environment, heat is propagated to the surroundings of the metallic structure through phonon-phonon (ph-ph) interaction from a few picoseconds to tens of nanoseconds [112, 113]. Simultaneously the hot-electron decay leads to plasmonic heating [114]. For plasmonic heating-based manipulation, the thermophoresis, Marangoni effect, and thermal convection are being studied and require further investigation [113].

Plasmon resonance energy transfer (PRET)

The spatial distribution of excited electrons and holes by the plasmonic resonance energy transfer (PRET) depends upon the electric field intensity (Scheme 7). It provides a root for the photocurrent where the carrier travels a smaller distance after photon absorption. PRET comes under indirect photocatalysis, where the distribution of excited electrons is similar to photoexcitation. PRET probability increased for metal nanoparticles with a combination of elastic dephasing, radiative, and non-radiative decay. As a result, it provides an enhanced electric field intensity in a small, well-defined semiconductor region. If the metal nanoparticle on the surface of the semiconductor forms localized states by Fermi-level pinning, it would cause more band bending by forming an energy barrier between e^- and h^+ [50].

Direct electron transfer (DET)

Direct electron transfer (DET) forms the electron-hole pairs directly independent of the light absorption characteristics of the semiconductor. Energy is considered to be stored in plasmon either by hot electrons or the local electric field. Electrons with energy spreading on LSPR peak wavelength stimulate hot electrons by oscillation. These oscillations are damped rapidly by radiative scattering due to the emission of photon or non-radiative electron-phonon and electron-electron scattering. Hot electrons with energy proportionate to the incident photons', overcome the energetically unfavorable Schottky barrier at the hetero-junction (Scheme 7) [115].

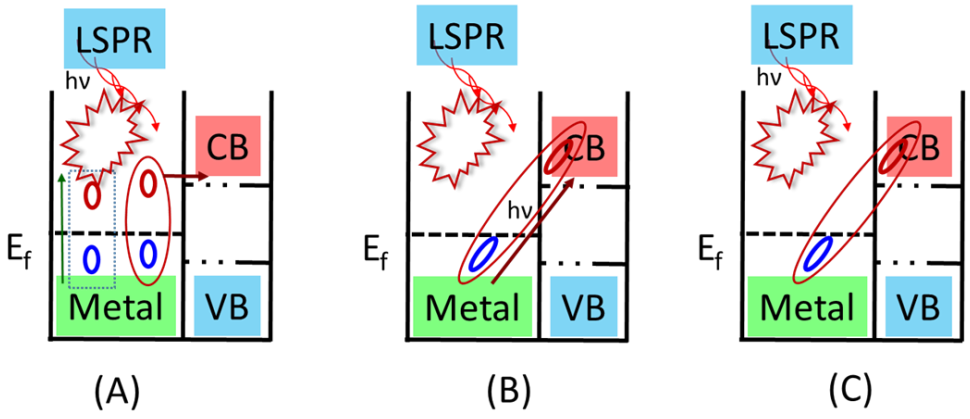

Scheme 7. Schematic representation of hot electron transfer process in (A) Plasmon-induced hot-electron transfer mechanism. (B) Direct metal-to-semiconductor interfacial charge-transfer transition mechanism. (C) Plasmon-induced metal-to-semiconductor interfacial charge-transfer transition mechanism [116]

Plasmon-induced resonance energy transfer (PIRET)

For Plasmon-induced resonance energy transfer (PIRET), the plasmonic enhancement depends upon the spectral overlap and does not require physical contact or electronic alignment for electron transfer, unlike DET [115]. The non-radiative hot electrons are transferred even the TiO_2 and AuNP are separated by an insulator [108, 117]. The electrons and holes are excited directly through the non-radiative relaxation of the localized surface plasmon dipole above and below the bandgap [118, 119]. The largest enhancement occurs when plasmon dephasing is closer to the semiconductor and overlaps with the band edge due to strong coupling to the weak band edge states (Scheme 7) [119]. The strength of PIRET depends upon the overlap of semiconductor's band edge (absorption band) with the LSPR resonance band, as well as the distance between the plasmonic metal and semiconductor dipole. There are suggestions that DET and PIRET can exist depending upon material parameters when charge transfer creates undesirable effects, such as carrier equilibration issues or material degradation [115].

Remote activity mechanism

In the 'remote activity mechanism,' photocatalysis starts degrading the dye touching the surface [120-122]. A ZnO combined TiO_2 film with AuNP causes remote oxidation of polyvynilydenefluoride films on octadecyltriethoxyl modified glass surface [121]. It is proposed that the active species from the film's surface migrate to the substrate by water and oxygen in the gas phase (Scheme 8).

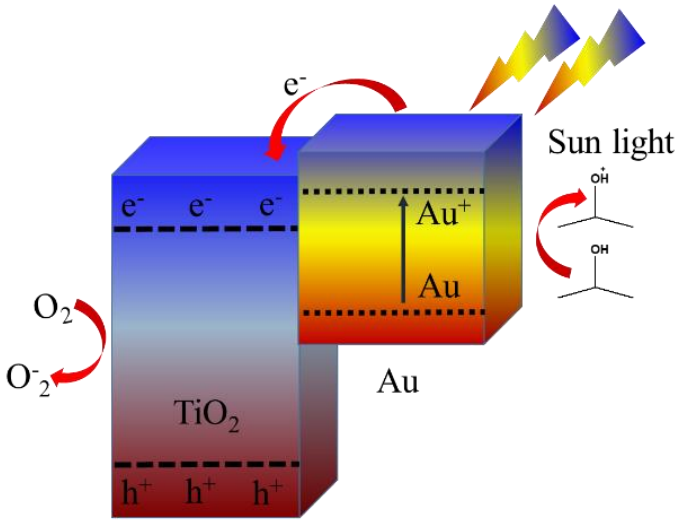

Scheme 8. Proposed remote activity mechanism in Au/TiO_2 [120]

Charge transfer mechanism

Charge separation in excited AuNP is explained by photoresponse spectrum coincidence with the surface plasmon absorption band [60, 120] (Scheme 7). Charge separation in AuNP/ TiO_2 provide oxidation potential for AuNP and reduction potential for TiO_2 [97, 120]. For TiO_2, electron diffusion is faster than hole migration due to charge jumping to the neighboring sites [120]. Transfer of e-s produces more efficient charge separation due to the surface barrier between AuNP and TiO_2 and reduces charge recombination [120]. A shift in the Fermi level towards more negative

potential increases energetics, enhancing the charge transfer process . AuNP tends to undergo quantization, and the charge equilibrates with the Fermi level [91]. For, this type of mechanism, the e-s are transferred from TiO_2 to AuNP if the concentration of AuNP is higher due to hindering the LSPR-promoted electron transfer [36, 91]. Consequently, AuNP causes string and shuttling of electrons in the photocatalytic process. The Fermi level of a semiconductor could be directly related to the number of electrons on the surface by the relation [91]:

$$E_F = E_{CB} + ktlnn_c/N_c \quad (2)$$

E_{CB}: conduction band energy level versus NHE

n_c: density of accumulated electrons

N_c is the charge carrier density of the semiconductor

Shifting of AuNP Fermi lFevel towards more negative potential leads to a move towards the TiO_2 CB due to more significant electron accumulation. A shift of the Fermi level improves the interfacial charge-transfer process and better the reduction ability [91, 123].

Plasmonic heating and hot electron transfer

Due to strong electron-phonon coupling in the metal nanoparticle, plasmon thermalizes itself for a few picoseconds. It results in a large introduction of electrons in TiO_2 [50, 92]. Femtosecond spectroscopy study of hot electrons takes 240 fs for electron injection, and therefore, many concluded that it is impossible to determine the mechanism of the hot electron injection [50, 124]. Electron-phonon coupling causes an increase in the lattice temperature, which modifies itself with the equilibrium size of the particles by $\Delta R/R = R\Delta T_l/3$, where R is the coefficient for thermal expansion.

Electrons generate high 'hot electron pressure' on the nuclei at higher temperatures. The contribution of this hot electron pressure to the expansion factor could be given by,

$$\alpha = {}^{1}/_{B}\left(\lambda C_1 + {}^{2}/_{3}\, C_e(T_e)\right) \quad (3)$$

where C_e and C_l are the electronic and lattice heat capacities, T_e is electronic temperature, B is the bulk modulus, and λ is the Gruneisen parameter for lattice.

From equation (3), first term on the right-hand side talks of lattice contribution to expansion, and the second term is associated with hot electron pressure. As for a non-spherical AuNP, multiple vibrational modes would be excited along different dimensions to contribute to elevate hot-electron pressure [109]. Dephasing of plasmon resonance either by the intrinsic damping processes of metal nanoparticles or by electron surface scattering causes photon absorption. This absorption of photons leads to the excitation of electrons spread over different levels in CB. This excited electron quickly equilibrates by electron-electron scattering in a few hundred femtoseconds, creating hot electron distribution. The hot electrons' distribution relaxes through phonon emission within a few picoseconds. Such coupling between the phonon modes and the hot electrons could be expressed by the two-temperature model (TTM). The rate of energy exchange between the phonons and electrons is given by,

$$C_e(T_e)\, dT_e / dT = -g(T_e - T_1) \quad (4)$$

Where T_e and T_l are the electronic and lattice temperatures accordingly;

C_l is lattice heat capacity, $C_e(T_e)=\gamma T_e$ is temperature-dependent electronic heat capacity, and g is electron-phonon coupling constant.

C_e is temperature-dependent,and the time required for electron-phonon coupling depends on initial electronic temperature [109].

Förster resonance energy transfer

If the radiative decay channel is negligible, all the light absorbed moves into hot carriers [12, 125]. The Förster resonance energy transfer (FRET) is where the excited state of the semiconductor is quenched by AuNP [50, 119]. Consequently, it is considered back reaction, does not involve any charge transfer, and occurs on a similar scale of PRET [50]. Although FRET does not involve the emission of any photon, donating the photoluminescence donor is critical for both quantum yield and emission spectrum [50]. The plasmonic dipole-dipole coupling takes place before Stoke's shift. It causes dephasing of the combined dipole moment and allows a red or a blue-shifted energy transfer by absorption and emission overlap. The plasmon initiates a population and moves to the semiconductor via PIRET, while the semiconductor leads to population transfer through FRET. If the dephasing of the semiconductor is faster than the plasmon, the largest PIRET transfer occurs. Thus, when PIRET becomes less effective, FRET turns stronger and, vice-versa [126-128].

Conclusion

The hot electrons are generated due to surface plasmon decay to the conduction band of TiO_2. To introduce new effective green catalysts, the separation of the electron-hole recombination by the hot carrier generation is the key. Efforts are being made for superior morphology control, novel hybrid structure, suitable energy coupling to achieve better efficiency and stability. To achieve this goal, further 'light' on understanding the hot electrons in AuNP/TiO_2 is essential. From this perspective, we reviewed and summarized the different parameters and proposals made on generating hot electrons and their roles. Based on current illustrative inquiries, there are several operating parameters such as size and shape, loading amount, irradiation wavelength, and crystalline phases of TiO_2, and the mechanism takes place in different ways, such as electron-phonon interaction, direct electron transfer, PRET, PIRET, remote activity, charge transfer, plasmon heating, Forster resonance energy transfer, etc. Future experiments will provide more insightful details on the effects of such parameters on the generation and the movement of the hot electrons in AuNP/TiO_2.

Abbreviations

Electron (e^-), hole (h^+), gold nanoparticle (AuNP), ultraviolet-visible (UV–vis), near-infrared (NIR), Valance band (VB), Conduction band (CB), Plasmon induced resonance energy transfer (PIRET), Förster resonance energy transfer (FRET)

Disclosure Statement

No potential conflict of interest was reported by the author.

Acknowledgments

The author declare that no funds, grants, or other support were received during the preparation of this manuscript therefore no acknowledgments do apply.

Orcid

Nasim Kamely : 0000-0002-7725-8806

References

[1]. Finkelmann H., Nishikawa E., Pereira G.G., Warner M. *Phys. Rev. Lett.*, 2001, **87**:015501 [CrossRef], [Google Scholar], [Publisher]

[2]. Redmond P.L., Brus L.E., *J. Phys. Chem. C* 2007, **111**:14849 [CrossRef], [Google Scholar], [Publisher]

[3]. Li Y., Guo Y., Long R., Liu D., Zhao D., Tan Y., Gao C., Shen S., Xiong Y., *Chinese J. Catal*., 2018, **39**:453 [Crossref], [Google Scholar], [Publisher]
[4]. Wu K., Chen J., McBride J.R., Lian T. *Science*, 2015, **349**:632 [Crossref], [Google Scholar], [Publisher]
[5]. Sousa-Castillo A., Comesaña-Hermo M., Rodríguez-González B., Pérez-Lorenzo M., Wang Z., Kong X.T., Govorov A.O., Correa-Duarte M.A. *J. Phys. Chem. C,* 2016, **120**:11690 [Crossref], [Google Scholar], [Publisher]
[6]. Costi R., Saunders A.E., Elmalem E., Salant A., Banin U. *Nano Lett*., 2008, **8**:637 [Crossref], [Google Scholar], [Publisher]
[7]. Li L., Wu B., Li G., Li Y. *RSC Adv*., 2016, **6**:28904 ([Crossref], [Google Scholar], [Publisher]
[8]. Molla A., Sahu M., Hussain S. *J. Mater. Chem. A*, 2015, **3**:15616 [Crossref], [Google Scholar], [Publisher]
[9]. Clavero C., *Nature Photon*., 2014, **8**:95 [Crossref], [Google Scholar], [Publisher]
[10]. Dai H., Yu Y., Wang X., Ma Z., Chen C., Zhou Z.-K., Han J., Han Y., Liu S.-D., Li L. *J. Phys. Chem.C*, 2015, **119**:27156 [Crossref], [Google Scholar], [Publisher]
[11]. Gieseking R.L., Ratner M.A., Schatz G.C., *Frontiers of Plasmon Enhanced Spectroscopy Volume 1*, American Chemical Society, 2016, **1245**, pp. 1-22 [Crossref], [Google Scholar], [Publisher]
[12] Manjavacas A., Liu J.G., Kulkarni V., Nordlander P. *ACS Nano*, 2014, **8**:7630 [Crossref], [Google Scholar], [Publisher]
[13]. Stockman M.I. in *Plasmonics: Theory and Applications*, edited by T. V. Shahbazyan and M. I. Stockman (Springer Netherlands, Dordrecht, 2013), pp. 1-101. [Google Scholar], [Publisher]
[14]. Maystre D., Lalanne P., Greffet J.J., Aizpurua J., Hillenbrand R., McPhedran R., Quidant R., Bouhelier A., Colas des Francs G., Grandidier J., Lerondel G., Plain J., Kostcheev S. *Plasmonics: From Basics to Advanced Topics*, 2012
[15]. Hartland G.V., Besteiro L.V., Johns P., Govorov A.O. *ACS Energy Lett.,* 2017, **2**:1641 [Crossref], [Google Scholar], [Publisher]
[16]. Hou W., Cronin S.B. *Adv. Funct. Mater*., 2013, **23**:1612 [Crossref], [Google Scholar], [Publisher]
[17]. Kamely N., Ujihara M. *J. Nanopart. Res.,* 2018, **20**:172 [Crossref], [Google Scholar], [Publisher]
[18]. Deng X.Q., Zhu B., Li X.S., Liu J.L., Zhu X., Zhu A.M. *Appl. Catal. B: Environ*., 2016, **188**:48 [Crossref], [Google Scholar], [Publisher]
[19]. Pany S., Naik B., Martha S., Parida K. *ACS Appl. Mater. Interfaces,* 2014, **6**:839 [Crossref], [Google Scholar], [Publisher]
[20]. Ujihara M., Imae T. *Colloids Surf. A Physicochem. Eng. Asp.*, 2013, **436**:380 [Crossref], [Google Scholar], [Publisher]
[21]. Ujihara M., Dang N.M., Imae T. *J. Nanosci. Nanotechnol*., 2014, **14**:4906 [Crossref], [Google Scholar], [Publisher]
[22]. Wu Y.H., Imae T., Ujihara M. *Colloids Surf. A Physicochem. Eng. Asp*., 2017, **532**:213 [Crossref], [Google Scholar], [Publisher]
[23]. Clavero C. *Nature Photon.,* 2014, **8**:95 [Crossref], [Google Scholar], [Publisher]
[24]. Ujihara M., Dang M.N., Imae T. *Sensors*, 2017, **17**:2563 [Crossref], [Google Scholar], [Publisher]
[25]. Li N., Zhao P., Astruc D. *Angew. Chem. Int. Ed.,* 2014, **53**:1756 [Crossref], [Google Scholar] [Publisher]
[26]. Louis C., Pluchery O. *Gold Nanoparticles for Physics, Chemistry and Biology*, World Scientific, 2017, pp. 51-85 [Google Scholar]

[27]. Malinsky D.M., Kelly K.L., Schatz G.C., Van Duyne R.P. *J. Phys. Chem. B*, 2001, **105**:2343 [Crossref], [Google Scholar], [Publisher]
[28]. Ayati A., Ahmadpour A., Bamoharram F.F., Tanhaei B., Mänttäri M., Sillanpää M. *Chemosphere*, 2014, **107**:163 [Crossref], [Google Scholar], [Publisher]
[29]. Hassan S.S., Solangi A.R., Agheem M.H., Junejo Y., Kalwar N.H., Tagar Z.A. *J. Hazard. Mater.*, 2011, **190**:1030 [Crossref], [Google Scholar], [Publisher]
[30]. Kamat P.V. *Pure Appl. Chem.*, 2002, **74**:1693 [Crossref], [Google Scholar], [Publisher]
[31]. Kamat P.V. *J. Phys. Chem. B*, 2002, **106**:7729 [Crossref], [Google Scholar], [Publisher]
[32]. Kowalska E., Remita H., Colbeau-Justin C., Hupka J., Belloni J. *J. Phys. Chem. C*, 2008, **112**:1124 [Crossref], [Google Scholar], [Publisher]
[33]. El-Kemary M., Abdel-Moneam Y., Madkour M., El-Mehasseb I. *J. Luminescence*, 2011, **131**:570 [Crossref], [Google Scholar], [Publisher]
[34]. Barakat T., Rooke J.C., Genty E., Cousin R., Siffert S., Su B.L., *Energy Environ. Sci.*, 2013, **6**:371 [Crossref], [Google Scholar], [Publisher]
[35]. Fan W., Leung K.M. *Molecules* 2016, **21**:180 [Crossref], [Google Scholar], [Publisher]
[36] Panayotov D.A., Morris J.R. *Surf. Sci. Rep.*, 2016, **71**:77 [Crossref], [Google Scholar], [Publisher]
[37]. Weon S., He F., Choi W. *Environ. Sci.: Nano*, 2019, **6**:3185 [Crossref], [Google Scholar], [Publisher]
[38]. Wang C., Astruc D. *Chem. Soc. Rev.*, 2014, **43**:7188 [Crossref], [Google Scholar], [Publisher]
[39]. Liu E., Fan J., Hu X., Hu Y., Li H., Tang C., Sun L., Wan J., *J. Mater. Sci.*, 2015, **50**:2298 [Crossref], [Google Scholar], [Publisher]
[40]. Kowalska E., Rau S., Ohtani B. *J. Nanotechnology*, 2012, **2012**:361853 [Crossref], [Google Scholar], [Publisher]
[41]. Wu Y., Liu H., Zhang J., Chen F. *J. Phys. Chem. C*, 2009, **113**:14689 [Crossref], [Google Scholar], [Publisher]
[42]. Gomathi Devi L., Kavitha R. *Appl. Surf. Sci.*, 2016, **360**:601 [Crossref], [Google Scholar], [Publisher]
[43]. Tung R. *Mater. Sci. Eng. R Rep.*, 2001, **35**:1 [Crossref], [Google Scholar], [Publisher]
[44]. Yogi C., Kojima K., Takai T., Wada N. *J. Mater. Sci.*, 2008, **44**:821 [Crossref], [Google Scholar], [Publisher]
[45]. Wang X., Caruso R.A. *J. Mater. Chem.*, 2011, **21**:20 [Crossref], [Google Scholar], [Publisher]
[46]. Celebi N., Aydin M.Y., Soysal F., Ciftci Y.O., Salimi K. *J. Alloys Compd.*, 2021, **860**:157908 [Crossref], [Google Scholar], [Publisher]
[47]. Dozzi M.V., Saccomanni A., Selli E. *J. Hazard. Mater.*, 2012, **211-212**:188 [Crossref], [Google Scholar], [Publisher]
[48]. Min B.K., Heo J.E., Youn N.K., Joo O.S., Lee H., Kim J.H., Kim H.S. *Catal. Commun.*, 2009,**10**:712 [Crossref], [Google Scholar], [Publisher]
[49]. Zhu J., Chen F., Zhang J., Chen H., Anpo M. *J. Photochem. Photobiol. A: Chem.*, 2006, **180**:196 [Crossref], [Google Scholar], [Publisher]
[50]. Warren S.C., Thimsen E. *Energy Environ. Sci.*, 2012, **5**:5133 [Crossref], [Google Scholar], [Publisher]
[51]. Linic S., Aslam U., Boerigter C., Morabito M. *Nature Mater.*,2015, **14**:567 [Google Scholar]
[52]. Wolfram H., Wriedt T. *The Mie Theory Basics and Applications*. Springer, 2012 [Google Scholar]

[53]. Sellappan R., Nielsen M.G., González-Posada F., Vesborg P.C.K., Chorkendorff I., Chakarov D., *J. Catal*. 2013, **307**:214 [Crossref], [Google Scholar], [Publisher]
[54]. Lin Z., Wang X., Liu J., Tian Z., Dai L., He B., Han C., Wu Y., Zeng Z., Hu Z. *Nanoscale*, 2015, **7**:4114 [Crossref], [Google Scholar], [Publisher]
[55]. Taghinejad M., Xu Z., Lee K.T., Lian T., Cai W. *Phys. Rev. Lett*., 2020, **124**:013901 [Crossref], [Google Scholar], [Publisher]
[56]. Kamely N. *J. Electron. Mater*., 2022, **51**:953 [Crossref], [Google Scholar], [Publisher]
[57]. Bouhadoun S., Guillard C., Dapozze F., Singh S., Amans D., Bouclé J., Herlin-Boime N. *Appl. Catal. B: Environ*., 2015, **174-175**:367 [Crossref], [Google Scholar], [Publisher]
[58]. Gołąbiewska A., Malankowska A., Jarek M., Lisowski W., Nowaczyk G., Jurga S., Zaleska-Medynska A. *Appl. Catal. B: Environ*., 2016, **196**:27 [Crossref], [Google Scholar], [Publisher]
[59]. Verbruggen S.W., *J. Photochem. Photobiol. C: Photochem. Rev*., 2015, **24**:64 [Crossref], [Google Scholar], [Publisher]
[60]. Tian Y., Tatsuma T. *J. Am. Chem. Soc*., 2005, **127**:7632 [Crossref], [Google Scholar], [Publisher]
[61]. Jin Z., Wang Q., Zheng W., Cui X. *ACS Appl. Mater. Interfaces*, 2016, **8**:5273 [Crossref], [Google Scholar], [Publisher]
[62]. Kelly K.L., Coronado E., Zhao L.L., Schatz G.C. *J. Phys. Chem. B,* 2003, **107**:668 [Crossref], [Google Scholar], [Publisher]
[63]. Gomes Silva C., Juárez R., Marino T., Molinari R., García H. *J. Am. Chem. Soc.*, 2011, **133**:595 [Crossref], [Google Scholar], [Publisher]
[64]. Kowalska E., Abe R., Ohtani B. *Chem. Commun*., 2009, 241 [Crossref], [Google Scholar], [Publisher]
[65]. Zhang H., Govorov A.O. *J. Phys. Chem. C,* 2014, **118**:7606 [Crossref], [Google Scholar], [Publisher]
[66]. Song C.K., Baek J., Kim T.Y., Yu S., Han J.W., Yi J. *Appl. Catal. B: Environ*., 2016, **198**:91 [Crossref], [Google Scholar], [Publisher]
[67]. Aravind P., de Jong W. *Prog. Energy Combust. Sci.*, 2012, **38**:737 [Crossref], [Google Scholar], [Publisher]
[68]. Shaikhutdinov S. *Gold Nanoparticles for Physics, Chemistry and Biology*, Imperial College Press: London, 2012, pp. 199-231 [Google Scholar]
[69]. Kiyonaga T., Jin Q., Kobayashi H., Tada H. *Chem. Phys. Chem*. 2009, **10**:2935 [Crossref], [Google Scholar], [Publisher]
[70]. Okazaki K., Morikawa Y., Tanaka S., Tanaka K., Kohyama M. *Phys. Rev. B*, 2004, **69**:235404 [Crossref], [Google Scholar], [Publisher]
[71]. Bian Z., Tachikawa T., Zhang P., Fujitsuka M., Majima T. *J. Am. Chem. Soc*., 2014, **136**:458 [Crossref], [Google Scholar], [Publisher]
[72]. Wang H., You T., Shi W., Li J., Guo L. *J. Phys. Chem. C*, 2012, **116**:6490 [Crossref], [Google Scholar], [Publisher]
[73]. Knight M.W., Sobhani H., Nordlander P., Halas N.J. *Science***,** 2011, **332**:702 [Crossref], [Google Scholar], [Publisher]
[74]. Quidant R., Louis C., Pluchery O. *Optical and Thermal Properties of Gold Nanoparticles for Biology and Medicine*, 2012, pp. 273-298 [Google Scholar]
[75]. Wang H., Brandl D.W., Le F., Nordlander P., Halas N.J. *Nano Lett*., 2006, **6**:827 [Crossref], [Google Scholar], [Publisher]
[76]. Nehl C.L., Liao H., Hafner J.H. *Nano Lett*., 2006, **6**:683 [Crossref], [Google Scholar], [Publisher]
[77]. Kathryn M.M., Feng H., Seunghyun L., Peter N., Jason H.H. *Nanotechnology*, 2010, **21**:255503 [Crossref], [Google Scholar], [Publisher]

[78]. Su F., Wang T., Lv R., Zhang J., Zhang P., Lu J., Gong J. *Nanoscale*, 2013, **5**:9001 [Crossref], [Google Scholar], [Publisher]
[79]. Guerrero-Martínez A., Barbosa S., Pastoriza-Santos I., Liz-Marzán L.M. *Curr. Opin. Colloid Interface Sci.*, 2011, **16**:118 [Crossref], [Google Scholar], [Publisher]
[80]. Fang Y., Jiao Y., Xiong K., Ogier R., Yang Z.J., Gao S., Dahlin A.B., Käll M. *Nano Lett.*, 2015, **15**:4059 [Crossref], [Google Scholar], [Publisher]
[81]. Mühlschlegel P., Eisler H.J., Martin O.J.F., Hecht B., Pohl D.W. *Science*, 2005, **308**:1607 [Crossref], [Google Scholar], [Publisher]
[82]. Nishijima Y., Ueno K., Yokota Y., Murakoshi K., Misawa H. *J. Phys. Chem. Lett.*, 2010, **1**:2031 [Crossref], [Google Scholar], [Publisher]
[83]. Zhang G., Miao H., Hu X., Mu J., Liu X., Han T., Fan J., Liu E., Yin Y., Wan J. *Appl. Surf. Sci.*, 2017, **391**:345 [Crossref], [Google Scholar], [Publisher]
[84]. Wu B., Liu D., Mubeen S., Chuong T.T., Moskovits M., Stucky G.D. *J. Am. Chem. Soc.*, 2016, **138**:1114 [Crossref], [Google Scholar], [Publisher]
[85]. Ho K.H.W., Shang A., Shi F., Lo T.W., Yeung P.H., Yu Y.S., Zhang X., Wong K.y., Lei D.Y. *Adv. Funct. Mater.*, 2018, **28**:1800383 ([Crossref], [Google Scholar], [Publisher]
[86]. Graciani J., Nambu A., Evans J., Rodriguez J.A., Sanz J.F., *J. Am. Chem. Soc.*, 2008, **130**:12056 [Crossref], [Google Scholar], [Publisher]
[87]. Chen Q., Zhang Y., Zhang D., Yang Y. *J. Water Process Eng.*, 2017, **16**:14 [Crossref], [Google Scholar], [Publisher]
[88]. Tian B., Li C., Gu F., Jiang H. *Catal. Commun.*, 2009, **10**:925 [Crossref], [Google Scholar], [Publisher]
[89]. Wang J., Tafen D.N., Lewis J.P., Hong Z., Manivannan A., Zhi M., Li M., Wu N. *J. Am. Chem. Soc.*, 2009, **131**:12290 [Crossref], [Google Scholar], [Publisher]
[90]. Wu Y., Zhang J., Xiao L., Chen F. *Appl. Catal. B: Environ.*, 2009, **88**:525 [Crossref], [Google Scholar], [Publisher]
[91]. Subramanian V., Wolf E.E., Kamat P.V. *J. Am. Chem. Soc.*, 2004, **126**:4943 [Crossref], [Google Scholar], [Publisher]
[92]. Tan T.H., Scott J., Ng Y.H., Taylor R.A., Aguey-Zinsou K.F., Amal R. *ACS Catal.*, 2016, **6**:1870 [Crossref], [Google Scholar], [Publisher]
[93]. Gołąbiewska A., Malankowska A., Jarek M., Lisowski W., Nowaczyk G., Jurga S., Zaleska-Medynska A. *The effect of gold shape and size on the properties and visible light-induced photoactivity of Au-TiO2*, 2016 [Crossref], [Google Scholar], [Publisher]
[94]. Tian B., Zhang J., Tong T., Chen F. *Appl. Catal. B: Environ.*, 2008, **79**:394 [Crossref], [Google Scholar], [Publisher]
[95]. Hidalgo M.C., Maicu M., Navío J.A., Colón G. *J. Phys. Chem.* C, 2009, **113**:12840 [Crossref], [Google Scholar], [Publisher]
[96]. Awazu K., Fujimaki M., Rockstuhl C., Tominaga J., Murakami H., Ohki Y., Yoshida N., Watanabe T. *J. Am. Chem. Soc.*, 2008, **130**:1676 [Crossref], [Google Scholar], [Publisher]
[97]. Du L., Furube A., Yamamoto K., Hara K., Katoh R., Tachiya M. *J. Phys. Chem. C*, 2009, **113**:6454 [Crossref], [Google Scholar], [Publisher]
[98]. Huang J., Liu Y., Lu L., Li L. *Res. Chem. Intermed.*, 2012, **38**:487 [Crossref], [Google Scholar], [Publisher]
[99]. Orlov A., Jefferson D.A., Macleod N., Lambert R.M., *Catal. Lett.*, 2004, **92**:41 [Crossref], [Google Scholar], [Publisher]
[100]. Oros-Ruiz S., Pedraza-Avella J.A., Guzmán C., Quintana M., Moctezuma E., del Angel G.,

Gómez R., Pérez E. *Top. Catal.,* 2011, **54**:519 [Crossref], [Google Scholar], [Publisher]
[101]. Ueno K., Misawa H. *NPG Asia Mater.*, 2013, **5**: e61 [Crossref], [Google Scholar], [Publisher]
[102]. Shuang S., Lv R., Xie Z., Zhang Z. *Sci. Rep*., 2016, **6**:26670 [Crossref], [Google Scholar], [Publisher]
[103]. Wang X., Long R., Liu D., Yang D., Wang C., Xiong Y. *Nano Energy*, 2016, **24**:87 [Crossref], [Google Scholar], [Publisher]
[104]. Priebe J.B., Radnik J., Lennox A.J.J., Pohl M.M., Karnahl M., Hollmann D., Grabow K., Bentrup U., Junge H., Beller M., Brückner A. *ACS Catal*., 2015, **5**:2137 [Crossref], [Google Scholar], [Publisher]
[105]. Mattesini M., Almeida J., Dubrovinsky L., Dubrovinskaia N., Johansson B., Ahuja R. *Phys. Rev. B*, 2004, **70**:212101 [Crossref], [Google Scholar], [Publisher]
[106]. Kimura K., Naya S.I., Jin-nouchi Y., Tada H. *J. Phys. Chem. C*, 2012, **116**:7111 [Crossref], [Google Scholar], [Publisher]
[107]. Yu M., Trinkle D.R. *J. Phys. Chem. C*, 2011, **115**:17799 [Crossref], [Google Scholar], [Publisher]
[108]. Jiang R., Li B., Fang C., Wang J. *Adv. Mater*., 2014, **26**:5274 [Crossref], [Google Scholar], [Publisher]
[109]. Hartland G.V. *Chem. Rev*., 2011, **111**:3858 [Crossref], [Google Scholar], [Publisher]
[110]. Sarina S., Waclawik E.R., Zhu H. *Green Chem*., 2013, **15**:1814 [Crossref], [Google Scholar], [Publisher]
[111]. Adleman J.R., Boyd D.A., Goodwin D.G., Psaltis D. *Nano Lett*., 2009, **9**:4417 [Crossref], [Google Scholar], [Publisher]
[112]. Palpant B. *Gold Nanoparticles for Physics, Chemistry and Biology*, Imperial College Press, 2011, pp. 75-102
[113]. Mascaretti L., Naldoni A. *J. Appl. Phys*., 2020, **128**:041101 [Crossref], [Google Scholar], [Publisher]
[114]. Bora T., Zoepfl D., Dutta J. *Sci. Rep.*, 2016, **6**:26913 [Crossref], [Google Scholar], [Publisher]
[115]. Cushing S.K., Wu N. *Electrochem. Soc. Interface*, 2013, **22**:63 [Crossref], [Google Scholar], [Publisher]
[116]. Lin S., Lu Y., Xu J., Feng S., Li J. *Nano Energy*, 2017, **40**:122 [Crossref], [Google Scholar], [Publisher]
[117]. Schuller J.A., Barnard E.S., Cai W., Jun Y.C., White J.S., Brongersma M.L. *Nature Mater*., 2010, **9**:368 [Crossref], [Google Scholar], [Publisher]
[118]. Ueno K., Misawa H. *J. Photochem. Photobiol. C: Photochem. Rev*., 2013, **15**:31 [Crossref], [Google Scholar], [Publisher]
[119]. Li J., Cushing S.K., Meng F., Senty T.R., Bristow A.D., Wu N., *Nature Photonics*, 2015, **9**:601 [Crossref], [Google Scholar], [Publisher]
[120]. Primo A., Corma A., Garcia H. *Phys. Chem. Chem. Phys.*, 2011, **13**:886 [Crossref], [Google Scholar], [Publisher]
[121]. Kubo W., Tatsuma T. *J. Mater. Chem.*, 2005, **15**:3104 [Crossref], [Google Scholar], [Publisher]
[122]. Han Z., Fei J., Li J., Deng Y., Lv M., Zhao J., Wang C., Zhao X. *Chem. Eng. J*., 2021, **407**:127214 [Crossref], [Google Scholar], [Publisher]
[123]. Shehzad N., Tahir M., Johari K., Murugesan T., Hussain M. *J. CO2 Util*., 2018 **26**:98 [Crossref], [Google Scholar], [Publisher]
[124]. Radzig M., Koksharova O., Khmel I., Ivanov V., Yorov K., Kiwi J., Rtimi S., Tastekova E., Aybush A., Nadtochenko V. *Nanomaterials*,

2019, **9**:217 [Crossref], [Google Scholar], [Publisher]
[125]. Furube A., Hashimoto S. *NPG Asia Mater.,* 2017, **9**:e454 [Crossref], [Google Scholar], [Publisher]
[126]. Becker P.C., Fragnito H.L., Cruz C.H.B., Fork R.L., Cunningham J.E., Henry J.E., Shank C.V. *Phys. Rev. Lett*., 1988, **61**:1647 [Crossref], [Google Scholar], [Publisher]
[127]. Sadeghi S.M. *Phys. Rev. A,* 2013, **88**:013831 [Crossref], [Google Scholar], [Publisher]
[128]. Zhang W., Govorov A.O., Bryant G.W. *Phys. Rev. Lett*., 2006, **97**:146804 [Google Scholar]

How to cite this manuscript: Nasim Kamely *. Hot Electron in Visible-Light-Induced Plasmonic Photocatalysis by AuNP/TiO_2 - A Review. *Journal of Medicinal and Nanomaterials Chemistry*, 5(1) 2023, 33-52. DOI: 10.48309/JMNC.2023.1.3